Current Research in Food Science 10 (2025) 101003

Contents lists available at ScienceDirect

Current Research in Food Science

journal homepage: www.sciencedirect.com/journal/current-research-in-food-science

Effects of plasma-activated water on structural and functional properties of PSE-like chicken protein isolate

Ke Li, Yanfang Zhou, Chenyan Zhu, Manting Du, Bo Chen, Dianbo Zhao, Yanhong Bai *

Key Laboratory of Cold Chain Food Processing and Safety Control, Ministry of Education, College of Food and Bioengineering, Zhengzhou University of Light Industry, Zhengzhou, 450001, PR China

ARTICLE INFO

Handling Editor: Dr. Maria Corradini

Keywords:
Plasma-activated water
PSE-Like chicken
Protein isolation
Structural property
Functional features

ABSTRACT

Pale, soft and exudative (PSE)-like chicken meat is rich in high-quality proteins, however, due to the properties of PSE-like meat, the functional characteristics of PSE-like chicken meat protein isolate (PPI) are affected. The present investigation aimed to improve the functional properties of PPI by employing plasma activation water (PAW), with the ultimate goal of enhancing its utility in various applications. The effects of PAW on the structure and function of PPI were evaluated. PAW treatment induced the protein structure to change from random coil to α-helix, which made the protein conformation more stable. PAW caused the hydrophobic residues to be exposed, thereby effectively enhancing their surface hydrophobicity. Dynamic rheology revealed the storage modulus of PPI gradually raised with increasing of PAW activation time. The scanning electron microscopy (SEM) showed that PAW promoted PPI to form a rough surface. When PAW activation time increased to 40 s, the foaming ability of PPI was raised by 77.84%, the emulsifying activity index was increased to 20.94 m^2/g, the emulsion stability index was improved by 20.40%, and the *in vitro* digestibility was increased by 25.15% ($P < 0.05$). The above results showed PAW could modify the structural properties, and effectively improve the emulsifying and foaming properties of PPI, and increase the *in vitro* digestibility of PPI.

1. Introduction

Pale, soft and exudative (PSE)-like chicken protein isolate (PPI) is a malfunctioning meat in meat, formed due to post-mortem heat stress (Gao et al., 2023). PSE-like chicken meat has a high incidence, leading to protein denaturation and excessive exudate loss, significantly influences the sensory quality of the product, decreases the quantity of meat products, and causing substantial economic losses to the meat-processing industry (Yang et al., 2021). Owens et al. (2000) concluded that PSE-like problems could cost the U.S. poultry meat industry more than 200 million dollars per year in economic losses. Carvalho et al. (2014) also predicted that losses to the Brazilian poultry meat industry could reach 5.1 million dollars per year due to increased juice losses of 5–10% in PSE-like turkeys. Although the quality of PSE chicken breast is damaged, its high protein content and rich variety are still an excellent source of protein nutrition (Zhao et al., 2020). Therefore, how to effectively process and utilize PPI is the focus of research.

Plasma is a green and environmentally friendly non-thermal processing new technology, consisting of various components such as free radicals, neutral particles, positive ions, and electrons, it can change the structure of proteins and effectively purify food and extend shelf life. (Farooq et al., 2023). Plasma has been used by a number of researchers for food purposes. Luo et al. (2022) found that pork's tenderness and water retention were improved using cold plasma treatment. Jiang et al. (2023) discovered that atmospheric pressure plasma jet may enhance the proteins cross-linking of in the myofibrillar protein of mandarin fish. Nevertheless, the direct application of plasma devices to food product surfaces may result in excessive protein oxidation and the accumulation of reaction substances on the surface area, posing challenges for handling large volumes and food products with uneven surface textures (Hadinoto et al., 2023). Meanwhile, plasma activated water (PAW) treatment is to place a sample into plasma activated water for full reflection, and in addition, PAW has reactive oxygen and nitrogen as well as low pH characteristics that will inactivate the microorganisms (Jadhav and Annapure, 2021). Li et al. discovered an increased surface hydrophobicity of chicken myofibrillar protein treated with PAW (Li et al., 2024). Kang et al. (2019) investigated the brightness of PAW-treated chicken breast increased with decreasing a* and b* values.

This article is part of a special issue entitled: Food physics published in Current Research in Food Science.

* Corresponding author. Ke Xue Road NO. 136, Zhengzhou, 450001, PR China.
E-mail addresses: xc_like@163.com (K. Li), baiyanhong212@163.com (Y. Bai).

https://doi.org/10.1016/j.crfs.2025.101003
Received 31 August 2024; Received in revised form 31 December 2024; Accepted 13 February 2025
Available online 14 February 2025

Liao et al. (2020) reported that PAW didn't influence the odor or texture of beef. Currently, PAW have been shown to maintain the organoleptic characteristics and affect the conformation of proteins. Dabade et al. (2023) discovered atmospheric pressure plasma increased the digestibility of soybean isolate protein. Wang et al. (2024) revealed an improved digestibility of chickpea isolate proteins by plasma treatment. Hence, this processing technique not only impacts the functionality but also affecting the nutritional value of proteins (Mollakhalili-Meybodi et al., 2021). Although this technique was used for the research of plant proteins and normal meat proteins, there is a lack of research concerning the structural and functional characterization of PSE-like chicken.

The study took PPI as the subject, investigating the impact of PAW on PPI by examining its structural, functional, and digestibility properties from multiple perspectives. The research assessed how PAW effects the primary, secondary, tertiary structures, emulsification activity index (EAI), emulsion stability index (ESI), Turbiscan stability index (TSI), and *in vitro* protein digestibility (IVPD) of PPI.

2. Materials and methods

2.1. Materials

The chicken breast meat came from a poultry company located in Henan Province (Zhengzhou, China). PSE-like chicken breasts (L*>53, $pH_{24\ h} < 5.7$) was carefully selected, stripped of fat and connective tissue, and then cut into small pieces (approximately $2 \times 2 \times 2\ cm^3$). They were mixed well (each bag was 100 g) and stored in a frozen state (−20 °C) for use within one week. The soybean oil was supplied by Yihai Kerry Jinlong Goldfish Grain and Oil Food Co., Ltd. (Shanghai, China). NaCl, NaOH, HCl, Na_2HPO_4, and NaH_2PO_4 were taken from Sinopharm Chemical Reagents Co., Ltd. (Shanghai, China), trypsin and chymotrypsin were sourced from Shanghai Yuanye Bio-Technology Co., Ltd. (Shanghai, China), and rhodamine dye was procured from Tianjin Kemio Chemical Reagents Co., Ltd. (Tianjin, China). All reagents employed in the experiment were analytically pure.

2.2. Extraction of PPI

Based on the approach of Li et al. (2023), 100 g sample was thawed at 4 °C for 12 h and subsequently processed into a paste using a pre-cooled meat grinder (GM 200, Restch Company, Germany) operating for 20 s at 2000 r/min, this process was repeated twice. Then, mixed the paste with deionized water in the ratio of 1:6 (m/V) at 4 °C and homogenized (UltraT25, IKA, Germany) for 2 min at 10,000 rpm. NaOH (2 M) was used to adjust the pH of the homogenate to 11 followed by cooling for 10 min at 4 °C to form a system of stable solutions. The above 150 mL solution was t subject to ultrasonication (VC750, Sonics, USA) at 450W for 10 min. After ultrasound, the solution was centrifuged at 10,000 rpm for 15 min at 4 °C, and the supernatant (containing soluble proteins) was used to adjust the pH value to 5.5 using 2 M HCl at 4 °C overnight. The protein was centrifuged for 15 min at 10,000 rpm, and the deposit (PPI) was gathered. The extracted protein was dissolved again in deionized water, modified to a final pH value of neutrality with 1 M NaOH, and finally lyophilized (Lab-1-50, Boiocool Experimental Instruments Co. LTD., China) to get PPI. The dried sample was stored in a self-sealing bag at −20 °C for further analysis.

2.3. Preparation of PAW

Using a low-temperature plasma jet generator (TS-PL200, Shenzhen Tonsontec Automation Equipment Co., Ltd, China) (Fig. 1) with a power of 750 W and a carrier gas pressure was 0.18–0.19 MPa, air was the excitation gas source. The air was pumped into the internal discharge chamber of the low-temperature plasma, where it reacted with a phosphate buffer solution (0.6 M NaCl, 20 mM Na_2HPO_4/NaH_2PO_4, pH = 7) (PBS) to generate PAW. The nozzle of the plasma jet was positioned on the 50 mL PBS about 4 cm and the plasma was jetted for 0–40 s (Control, PAW_{10}, PAW_{20}, PAW_{30}, and PAW_{40}). Three independent trials were conducted at various occasions. The PPI was subsequently diluted to 60 mg/mL with the proper amount of PAW (Control, PAW_{10}, PAW_{20}, PAW_{30}, and PAW_{40}) made of PBS and incubated for 12 h at 4 °C before use. Three independent trials were conducted at various occasions. In each trial, all five PAW preparation (Control, PAW_{10}, PAW_{20}, PAW_{30}, and PAW_{40}, respectively) and PPI dilutions were performed in triplicate. Each measurement was carried out at least in triplicate.

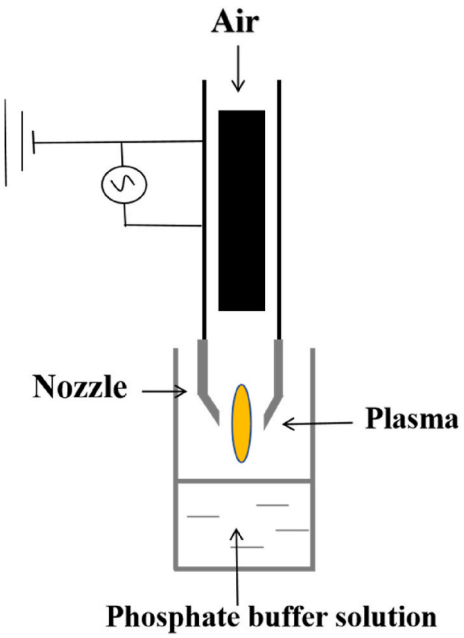

Fig. 1. Schematic diagram of plasma activated water preparation.

2.4. Sodium dodecyl sulfate-polyacrylamide gel electrophoresis (SDS-PAGE))

PPI solution was diluted to a concentration of 5 mg/mL with equal amount of PBS, and mixed it with the same volume of reducing buffer (0.5 M Tris-HCl, 20% Gly, 10% SDS, 3.33% DTT, and 2% bromophenol blue) or non-reducing buffer (0.5 M Tris-HCl, 20% Gly, 10% SDS, 2% bromophenol blue) at room temperature (RT). Then, boiled the mixture at 100 °C for 5 min. The electrophoresis gel consisted of 10% separating gel and 5% concentrated gel, with a loading volume of 10 μL. Electrophoresis was carried out a vertical electrophoresis device for 20 min at 60 V, then at 110 V for about 1.2 h. Staining with Commassie Brilliant Blue R-250 for 30 min. Then, decolorizing agent was used to decolorize it until the background became clear. Myosin and actin bands were quantitatively analyzed under reducing conditions by Quantity One software using gel imager (Bio-Rad, USA).

2.5. Secondary structure

Based on the approach outlined by Li et al. (2022a) with minor adjustments, secondary structure content of PPI was assessed with circular dichroism spectroscopy (Chirascan V100, Applied Photophysics, Leatherhead UK). PPI solution was diluted to a concentration of 0.1 mg/mL with equal amount of PBS. The bandwidth was 1 nm, response time was 0.25 s, scanning speed was 50 nm/min, and data collection over 190–260 nm wavelength range of were employed. CDNN software was utilized for the secondary structure content of PPI (0.1 mg/mL).

2.6. Surface hydrophobicity

The surface hydrophobicity of PPI was determined by referring to the way of Zhao et al. (2017) with minor changes. PPI solution was diluted to a concentration of 1 mg/mL with equal amount of PBS. Added about 80 μL of 0.1% bromophenol blue (BPB) solution into 1 mL of PPI (1 mg/mL) and incubated for 15 min at RT with intermittent shaking. The supernatant was collected by centrifugation for 10 min at 5000 rpm and collected. Diluted it 10 Times. Measured the absorbance at 595 nm, denoted as A_0. The background control involved diluting BPB without PPI solution by the same factor, denoted as A_1, while using PBS as a blank. The formula for calculating the amount of BPB bound was:

$$\mathrm{BPB}(\mu\mathrm{L}) = 80 \times \frac{A_1 - A_0}{A_1} \tag{1}$$

2.7. Fluorescence intensity

According to the approach by Zhao et al. (2018), the intrinsic fluorescence spectrum of PPI was determined with slight adjustments. PPI solution was diluted to a concentration of 1 mg/mL with equal amount of PBS and subjected to analysis by Fluorimeter (F-7000, Hitachi Crop., Japan). A quartz cuvette with a path length of 1 cm was employed, excitation wavelength of 280 nm, emission spectrum range spanning from 290 to 460 nm. Set the slit width to 5 nm for both excitation and emission, while the scanning speed was maintained at 12,000 nm/min.

2.8. Total sulfhydryl content

Determination of total sulfhydryl content by a way of Sharifian et al. (2019) with minor adjustments. PPI solution was diluted to a concentration of 5 mg/mL with equal amount of PBS. Subsequently, approximately 8 mL of urea SDS solution (comprising 3% SDS, 8.0 M urea, and 0.6 M NaCl at pH 7.0) was added to 2 mL of PPI (5 mg/mL) and agitated at RT for 5 min intermittently. Following this, the resulting mixture (5 mL) was thoroughly combined with DNTB (1 mg/mL) solution in a ratio of 5:1 and incubated at RT for 1 h before using a spectrophotometer to measure the absorbance value at 412 nm.

2.9. Turbidity and solubility

PPI solution was diluted to 1 mg/mL with equal amount of PBS, then measured the adsorption value at 660 nm to reflect turbidity. According to method of Eazhumalai et al. (2023), each PPI solution, which had been separated following treatment with control and PAW, was subjected to centrifugation at 10,000 r/min for 10 min at 4 °C. Subsequently, PPI concentration was determined using the biuret reagent. The solubility of proteins (%) was defined as the proportion of soluble proteins in the supernatant to the total proteins in the dispersion:

$$\mathrm{Solubility}(\%) = \frac{W_1}{W_2} \times 100 \tag{2}$$

Where W_1 denotes the protein concentration in the supernatant (%), W_2 denotes the initial protein concentration (%).

2.10. Particle size and zeta-potential

The particle size and Zeta-potential of PPI were determined following the approach of Zhao et al. (2022),. Each PPI solution was diluted to a concentration of 1 mg/mL with equal amount of PBS, and the average particle size and Zeta-potential were tested by laser particle size analyzer (Nano-ZS90, Malvern, Britain) at 25 ± 1 °C. The experimental parameters included a material refractive index of 1.52, with water as the medium, and a medium refractive index of 1.333.

2.11. Rheological properties

According to the method of Li et al. (2020a), dynamic rheology was assessed utilizing a rheometer equipped with a 40 mm parallel steel plate (TA, American). Each PPI solution (60 mg/mL) was hermetically sealed with silicone oil to mitigate water evaporation during testing. Experimental parameters were configured as follows: gap distance of 1 mm, strain of 1%, frequency of 0.1 Hz, and temperature ramped at a rate of 2 °C/min from 25 °C to 80 °C, while recording the storage modulus (G′).

2.12. Foaming capacity (FC)

The FC was determined by an approach described by Sharafodin et al. (Sharafodin and Soltanizadeh, 2022) with slight adjustments. Each PPI was diluted with a phosphate buffer solution to 10 mg/mL, then 10 mL of PPI solution was precisely transferred to a beaker and homogenized twice for 30 s at 10,000 r/min. The FC of PPI was calculated with the following formula:

$$\mathrm{FC}(\%) = \frac{V_1 - V_0}{V_0} \times 100 \tag{3}$$

Where V_0 is the volume of the non-sheared PPI solution, 10 mL, V_1 is the volume of the foam generated immediately after shearing.

2.13. Microstructure

PPI solution (60 mg/mL) was vacuum-frozen dried, both without PAW treatment and after PAW treatment. The scanning electron microscope (Regulus 8100, Hitachi, Japan) (SEM) operated under a 10.0 kV accelerating voltage and a magnification of 500 times for observing the microstructure of different samples after gold coating.

2.14. Emulsion preparation of PPI

Each PPI solution was diluted to a concentration of 10 mg/mL and then homogenized with soybean oil (m/V) at a ratio of 4:1 for 2 min at 10,000 rpm, and an emulsion containing PPI would be obtained.

2.14.1. Emulsifying activity index and emulsion stability index

In accordance with the methodology outlined by Wang et al. (2023), EAI and ESI were determined. 10 mL of a 10 mg/mL PPI solution was combined with 2.5 mL of soybean oil at a speed of 10,000 rpm and homogenized four times for 30 s each. At 0 min and 10 min following completion of emulsification, 50 μL of emulsion was promptly extracted and mixed with 5 mL of 0.1% SDS solution, and the absorbance at 500 nm was measured. The values for EAI and ESI were then calculated with the subsequent formula:

$$\mathrm{EAI}\left(\mathrm{m^2/g}\right) = \frac{2 \times 2.303 \times A_0 \times D}{C \times W \times 10000} \tag{4}$$

$$\mathrm{EAI}(\%) = \frac{A_0 \times 10}{A_0 - A_{10}} \times 100 \tag{5}$$

Where A_0 and A_{10} denote the absorbance at 500 nm wavelength for 0 min and 10 min, respectively, D represents the dilution factor, W represents the oil phase volume fraction (20%), and C represents the protein concentration (g/mL).

2.14.2. Turbiscan stability index

Taked 20 mL of fresh emulsion (10 mg/mL PPI emulsion) into a special sample bottle for Turbiscan stability analyzer (Formulation, Toulouse, France) and performed the test. The test procedure was to scan the sample every 60 s for a total of 1800 s.

2.15. In vitro simulated digestion

Following a way of Sun et al. (2022) with minor change, *in vitro* simulated digestion of PPI was conducted. Each PPI solution was diluted to a concentration of 10 mg/mL with PBS. Adjusted 10 mL of PPI solution (10 mg/mL) to pH 2.0 using 1 M HCl, then added 1 mL of pepsin solution (0.1 M HCl, 40 mg/mL), and then incubated (HT-100B, New Chunlan Scientific Instrument Co., LTD, Jiangsu, China) on a shaker (150 rpm) for 1 h at 37 °C for gastric digestion. Adjusted the pH of the gastric digesta using 1 M $NaHCO_3$ to 7.0 after gastric digestion. Subsequently, 1 mL trypsin solution (0.01 M PBS, 10 mg/mL) was added, then the mixture was further incubated on a shaker (150 rpm) for an additional 2 h at 37 °C for enteric digestion. Put the digested mixture into a boiling water bath for 10 min to terminate the digestion reaction, and then samples were prepared for analysis.

2.15.1. In vitro protein digestibility

Centrifuged the digestive samples at 8000 rpm at 4 °C for 10 min, and then absorb the supernatant. Protein content was determined using the biuret method, with the supernatant protein content as A and the total protein content of the sample as B, and calculated the according to the following formula.

$$\mathrm{IVPD}(\%) = \frac{A}{B} \times 100 \quad (6)$$

Where B denotes the protein content in the sample before digestion, measured in milligrams (mg), and A denotes the protein content in the supernatant, measured in milligrams (mg).

2.15.2. Laser microconfocal Raman spectrometer

By the way of Zhang et al. (2023), with slight modifications, the microstructures of digested products were measured with laser confocal Raman spectrometer. 1.0 mL digested sample was mixed with 20.0 μL of Rhodamine solution (water soluble, 0.1% w/v aqueous solution) and incubated to stain the protein phase for 15 min. Afterward, placed 5 μL of the stained sample in the center area of a microscope cover slip and carefully covered the coverslip to exclude air bubbles, and then use nail polish to seal along the edges. Observed the distribution and size of each sample.

2.16. Data statistical analysis

The data were expressed as the mean ± standard deviation. The data were analyzed by one-way ANOVA with SPSS 27.0 software, and multiple comparisons were made using Duncan's method. $P < 0.05$ was considered to be a significantly differences between the treatment groups and had statistical significance.

3. Results and discussion

3.1. SDS-PAGE

The impact of varying PAW activation durations on the weight of PPI molecules are illustrated in Fig. 2. In both reduced and non-reduced conditions, when PPI was subjected to varying PAW activation durations, the original protein feature bands remained unaltered, with no new protein bands appeared. This indicated there were no significant difference observed in the treated PPI compared to control group, and their structural integrity was preserved. Consequently, it can be deduced that PAW did not induce modifications in the primary structure of PPI (Li et al., 2022a). The alterations in the primary structure of PPI induced by PAW are not dominate. Rao et al. (2023) also observed that PAW did not change the characteristic bands of duck meat myofibrillar protein. However, with the increase of the activation time of PAW, the intensity of the bands of myosin heavy chain (MHC) and actin (AC) can be observed to gradually decrease both in the reduced and non-reduced conditions. This may be MHC and AC are two muscle proteins that are more easily oxidized, they are the main targets of oxidative reactions, and PAW promote oxidation that would induce cross-linking of MHC and AC and promote protein aggregation. (Baron et al., 2007; Olatunde et al., 2019). Baron et al. (2007) discovered that MHC and AC play crucial roles as key proteins in oxidative reactions, as MHC and AC are oxidized promoted, the generation and aggregation of polymeric bodies. Olatunde et al. (2019) observed a reduction of MHC and AC band intensity in Asian perch fillets with increasing plasma treatment time.

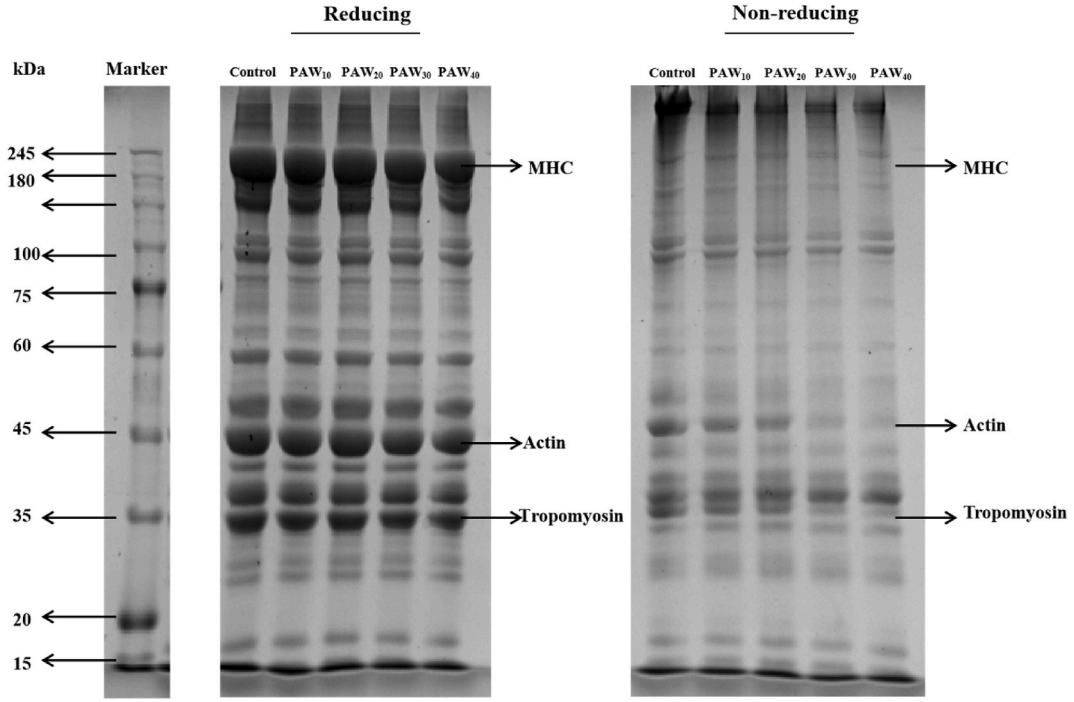

Fig. 2. Effects of plasma activation time on SDS-PAGE profile of PSE-like chicken protein isolate.

3.2. Secondary structure

Circular dichroism spectroscopy is commonly employed method to assess alterations in the secondary structure of proteins (Ekezie et al., 2019a). As shown in Fig. 3A, PAW-treated and control samples ($P < 0.05$) differed significantly in the secondary structure components between. With increasing PAW activation time, there was a concurrent increase in α-helix content and a decrease in random coil content ($P < 0.05$). After PAW treatment, PPI structure changed from a random coiled structure to an α-helix structure, which indicated that short time PAW activation treatment caused a conformational shift of PPI to a more stable and ordered secondary structure (Mehr and Koocheki, 2020). As the activation time of PAW was prolonged, the content of β-sheet gradually decreased ($P < 0.05$). Hydrogen bonds between peptide chains maintain β-sheet (Ekezie et al., 2019b). A reduction in β-sheet content implies that some of the hydrogen bonds stabilizing the structure have been broken, leading to conformational unfolding and loosening (Li et al., 2020b). Meanwhile, the reduction in the content of β-sheet indicates the hydrophobic sites within the molecule became exposed (Segat et al., 2016; Misra et al., 2016). Mehr et al. (Mehr and Koocheki, 2020) observed increasing α-helix content and decreasing random coil content of soybean isolate protein following plasma treatment, leading to enhanced stability in the protein conformation. Jiang et al. (2023) found that atmospheric pressure plasma-treated *Siniperca chuatsi* myofibrillar fibrillar proteins had an increased α-helix content while a decreased random curl content.

3.3. Surface hydrophobicity

The alteration in protein surface hydrophobicity is influenced by the number and spatial arrangement of hydrophobic residues on the surface of protein, and can reflect the alterations in the tertiary structure of proteins (Li et al., 2020b). Fig. 3B shows the effect of PAW on the hydrophobicity of PPI surface. With increasing PAW activation time, the binding capacity of BPB significantly enhanced from 17.02 μL to 48.51 μL ($P < 0.05$). This may be due to the powerful electrostatic repulsion induced by PAW between protein molecules, resulting in more noticeable unfolding and folding of proteins, increased exposure of hydrophobic regions on the protein surface, which consequently enhanced BPB binding to augment protein surface hydrophobicity (Wang et al., 2024). Jiang et al. (2023) discovered that the atmospheric plasma jet treatment (650 W, 0–12 s) of myofibrillar protein in mandarin fish could promote protein-protein interactions and induced alterations in the protein molecules tertiary structure, this process led to the exposure of internal cysteine groups and hydrophobic regions, consequently increasing the surface hydrophobicity.

3.4. Fluorescence intensity

Changes in the microenvironment of tryptophan residues can be reflected by intrinsic fluorescence of proteins (as part of the protein's tertiary structure) (Li et al., 2019; Zhang et al., 2018). As illustrated in Fig. 3C, the fluorescence intensity of PPI obviously decreased compared to the control group ($P < 0.05$) with increasing PAW activation time. PAW treatment led to fluorescence quenching of PPI. This was because by treating the protein with PAW, exposure of aromatic amino acid residue to a polar water environment, and some tyrosine and tryptophan residues may be oxidized and modified by compounds, including hydroxyl radicals and ozone (Sun et al., 2021; Ukai et al., 2008). Rao et al. (2023) observed that as the activation time of PAW increased, the fluorescence intensity of duck meat myofibrillar protein significantly decreased. It was consistent with the surface hydrophobicity results (Fig. 3B), indicating that the proteins reacted with the reactive compounds of PAW to expose more hydrophobic groups.

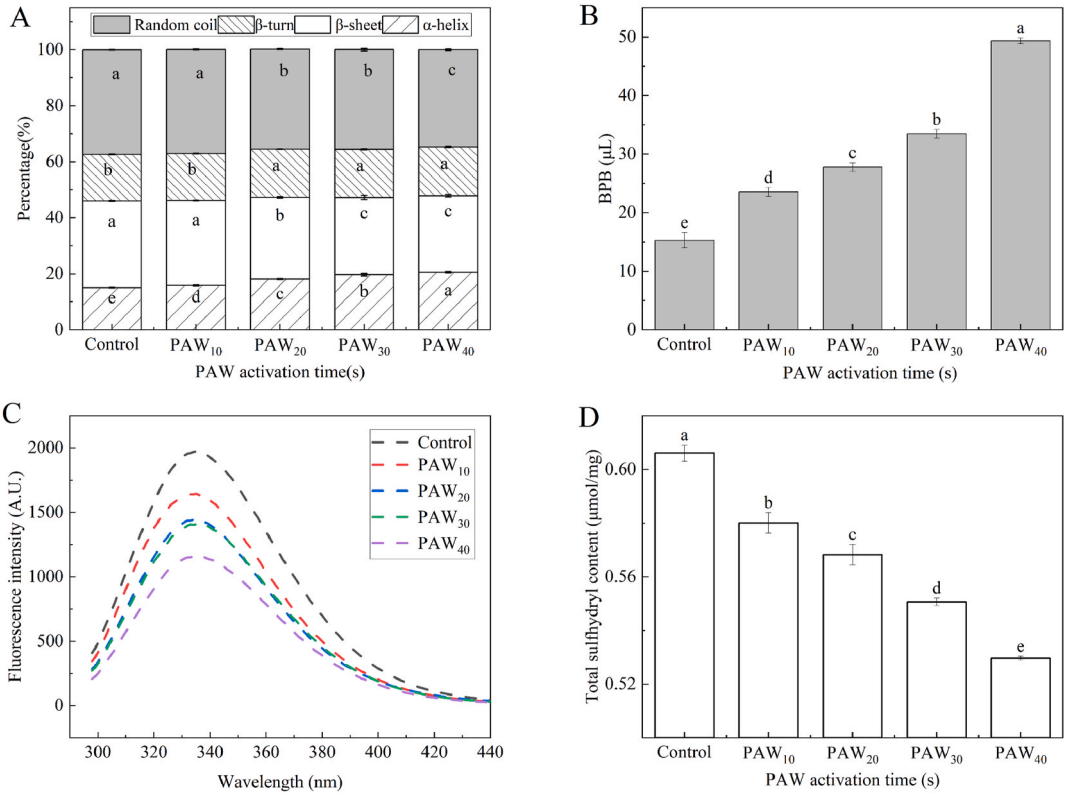

Fig. 3. Effect of plasma activation time on the secondary structure, surface hydrophobicity, fluorescence intensity and total sulfhydryl content of PSE-like chicken protein isolate. A: secondary structure, B: surface hydrophobicity, C: fluorescence intensity, D: total sulfhydryl content. Different letters (a–e) indicate significant differences ($P < 0.05$).

3.5. Total sulfhydryl content

Sulfhydryl is among the strongest reactive functional groups in proteins and regarded as indicator of oxidation, forming disulfide bonds under oxidizing conditions, leading to a decrease in its concentration (Ekezie et al., 2019b). Fig. 3D illustrates the variations in total sulfhydryl content of PPI following treatment with PAW. With the increase in PAW activation time, a gradual decrease in the total sulfhydryl content of PPI was observed. In comparison to the control, at PAW_{40}, the total sulfhydryl content was a significant reduced by12.61% ($P < 0.05$). This may be due to the PAW treatment exposed more hydrophobic groups, and consequently triggered protein interactions and aggregation, subsequently causing the exposed cysteines to be re-wrapped by the polymer collective, thereby reducing the total cysteine content (Liu et al., 2020; Miao et al., 2020). In other hand, plasma could accelerate the loss of cysteine sulfhydryl, which are exceptionally susceptible to ROS, cysteine and methionine contain sulfhydryl groups that are oxidized easily, bringing about the formation of intramolecular and intermolecular disulfide bonds, which reduce the total sulfhydryl content (Soladoye et al., 2015). Luo et al. (2022) found plasma treatment (50, 60, 70 kV) of pork myofibrillar protein would reduce the total content of cysteine.

3.6. Turbidity and solubility

Turbidity and solubility of protein reflect their degree aggregation. An increase in protein turbidity exhibits a strong positive correlation with a reduction in protein solubility. As the level of protein aggregation escalates, so does the turbidity value, while solubility diminishes (Wang et al., 2022a; Hatab et al., 2022). As shown in Fig. 4A, it illustrates the alterations in PPI turbidity and solubility following PAW treatment. As the duration of PAW activation increases, PPI's turbidity gradually rised while its solubility decreased progressively ($P < 0$ 0.05). Compared to control, turbidity rose by 17.67% and the solubility decreased to 16.20% at PAW_{40}. It may be because the ROS produced by PAW caused protein oxidation, leading to protein denaturation and precipitation, thus reducing the protein turbidity and increasing the solubility (Zhang et al., 2013). Additionally, protein molecules unfolded, exposing internal hydrophobic groups would interact and lead aggregation of protein, which in turn increase in turbidity and decrease in solubility (Wang et al., 2024; Zhang et al., 2021). Jiang et al. (2023) observed that exposure to atmospheric pressure plasma jet (0–12 s) led to a raise in turbidity and a reduce in the solubility of myofibrillar protein in guppy.

3.7. Particle size and zeta-potential

Particle size is frequently utilized for assessing the dimensions of protein aggregates. From Fig. 4B, it was evident that with the increase in activation time of PAW, there is a gradual increment in particle size ($P <$ 0.05). Compared to control, the particle size of PPI from PAW_{40} treatment increased by 33.31%. This may arise because the exposure of hydrophobic residues within PPI as a result of PAW treatment, leading to the unfolding of PPI secondary and tertiary structures, ultimately leading to the increased aggregation and particle size of PPI (Ekezie et al., 2019b). Qian et al. (2021) found that when chicken meat myofibrillar protein was treated with PAW, the myofibrillar protein was partially oxidized by ROS in PAW, causing the myofibrillar protein molecules to form disulfide bonds, and consequently augmenting particle size.

Fig. 4B also illustrates the variations in the zeta-potential of PPI following PAW treatment. With the PAW activation time increasing from 0 s to 40 s, protein zeta-potential shifted from an initial value of −3.98 mV to −6.90 mV, leading to a clear rise in the negative charge of PPI ($P < 0.05$). This is because the density of the chemical reactants in the plasma voltage was higher, which increased the oxidation of amino acid residues into negatively charged byproducts, thereby increasing the negative charge (Mehr and Koocheki, 2020). Therefore, PAW can be an

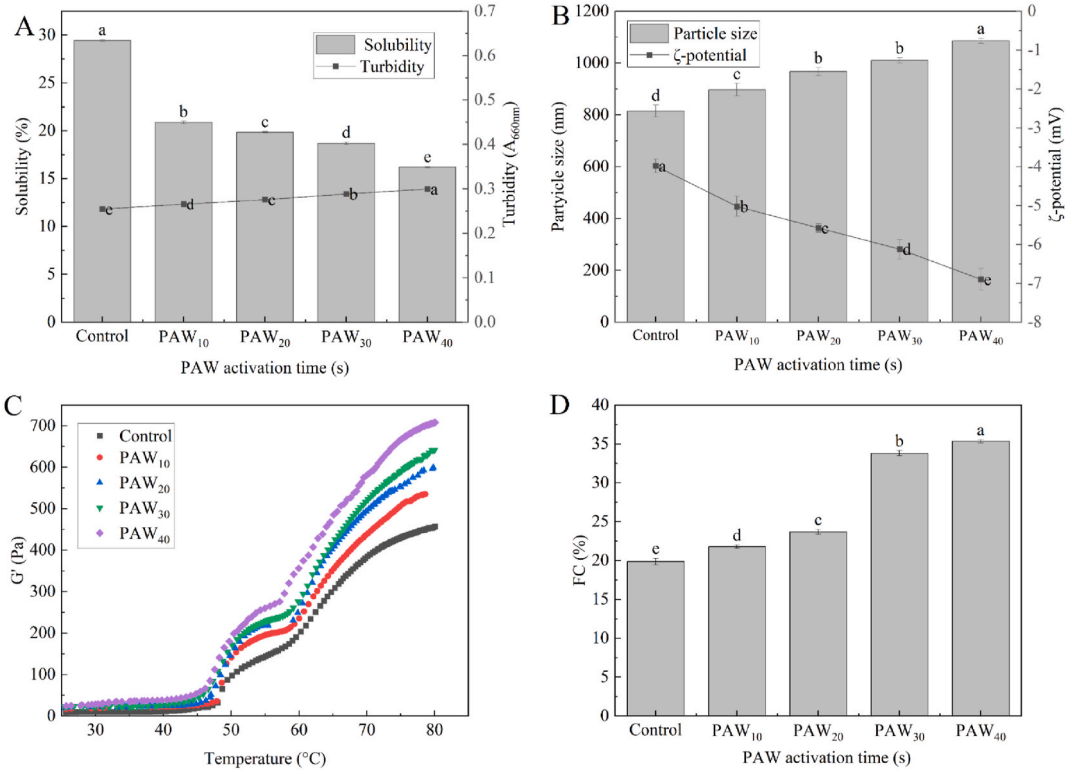

Fig. 4. Effect of plasma activation time on the solubility and turbidity, particle size and ζ-potential (B), storage modulus (G′) and foaming characteristic (FC) of PSE-like chicken protein isolate. A: solubility and turbidity, B: particle size and ζ-potential, C: storage modulus (G′), D: FC. Different letters (a–e) indicate significant differences ($P < 0.05$).

efficient way to enhance protein surface charge, thereby improving the stability by increasing the electrostatic repulsion of the emulsion between droplets.

3.8. Rheological properties

Fig. 4C illustrates the temperature-dependent variation of the storage modulus (G′) for PPI over a range from 25 °C to 80 °C. Between 25 and 45 °C, the G′ value of the treatment group tended to a flat pattern, when the temperature rose to 47–55 °C, G′ value increased linearly, which was the initial stage of gel network formation, when the temperature rose to 55–58 °C, G′ value exhibited a tendency to revert to a smooth pattern, within the temperature range of 57–80 °C, G′ value increased linearly for the second time. The second linear increase was due to permanent, irreversible cross-linking of myosin filaments by covalent disulfide bonds and hydrophobic interactions, at which point the sample system has formed a good three-dimensional gel network structure (Visessanguan et al., 2000). Among PPI samples, the G′ value at PAW_{40} exhibited the highest magnitude, whereas the un treated PPI demonstrated the lowest degree of elasticity. The results revealed that PAW improved the elasticity of PPI, which may be owing to the presence of substances with hydroxyl radicals and hydrogen peroxide in PAW, which caused oxidation of PPI and thus improve its elasticity (Xiong et al., 2010; Sarangapani et al., 2016). Additionally, the enhancement of gel elasticity might be connected to changes in protein cross-linking. During the gelation process of PPI subjected to PAW heating, the presence of oxidizing substances may oxidize the myosin tail disulfide bonds, making the myosin tail disulfide bonds cross-linking more stable than the head-to-head cross-linking of myosin heads in non-oxidizing conditions, ultimately facilitating the development of a stably gel structure for PPI gels (Park et al., 2007). Li et al. (2022b) also revealed that PAW could enhance the structural network of myofibrillar protein gel.

3.9. Foaming capacity

Protein foamability indicates its surface activity in water and its capacity to generate foam. As illustrated in Fig. 4D, as the PAW activation time increased, FC significantly increased ($P < 0.05$). The generation of ROS and RNS by plasma may induce the unfolding of amino acid side chains and oxidation of protein, thereby forming structural flexibility and generating better foam formation at the water-air interface (Wang et al., 2023). It was also possible that it was related to the hydrophobic groups becoming exposed, because PAW treatment further disrupted the protein's spatial structure, exposing hydrophobic groups, and allowed proteins to adsorb more readily to the air-water interface and trap air bubbles more efficiently (Wang et al., 2022b; Wierenga et al., 2003), which was the key reason for the FC increased. Yu et al. (2020) observed soybean protein subjected to plasma treatment (0–15 s) exhibited enhanced foaming properties.

3.10. Microstructure

SEM reflect the microscopic morphological changes and surface characteristics of proteins. The microstructures of PPI by different PAW activation times are illustrated in Fig. 5. The structure of PPI in the control displayed a relatively flat and smoother morphology with minimal wrinkles, in contrast to PPI in the PAW-treated group, which exhibits a notably increased roughness of surface. It was attributed to the impact of high-energy electrons generated in PAW on the protein surface, resulting in oxidation and the consequent formation of rough surface structure on the protein (Yu et al., 2022). Additionally, Yang et al. (2025) found PAW also led to the development of a rough surface structure on polysaccharides.

3.11. Emulsifying activity index and emulsion stability index

EAI and ESI assess the emulsifying efficiency and stability of the protein emulsion. As shown in Fig. 6A, PAW treatment could significantly enhance EAI and ESI of PPI. Compared to the control, the EAI of PPI was increased to 20.94 m^2/g, and the ESI was increased by 20.40% ($P < 0.05$) at the condition of PAW_{40}. This was probably attributed to the exposure of the protein's hydrophobic groups by PAW treatment, and causing its surface hydrophobicity to increase (Fig. 3B). Consequently, it enhanced the protein's surface activity and augmented its capacity to bind to oil droplets (Sharifian et al., 2019). It may also be related to the expansion of protein structure caused by PAW treatment, resulting in the exposure of hydrophobic amino acid residues and an augmentation in the conformational flexibility of the protein. This, in turn, improves surface activity at the oil-water interface and increases protein adsorption energy (Zhang et al., 2017). The impact of PAW on EAI and ESI was in line with the influence of hydrophobicity on the protein surface. The emulsifying ability of PAW_{40}-treated protein remained unimpaired, suggesting the oxidation of the protein induced by PAW_{40} may not compromise protein functionality. Sharafodin et al. (Sharafodin and Soltanizadeh, 2022) discovered plasma treatment of soybean isolates raised their EAI and ESI.

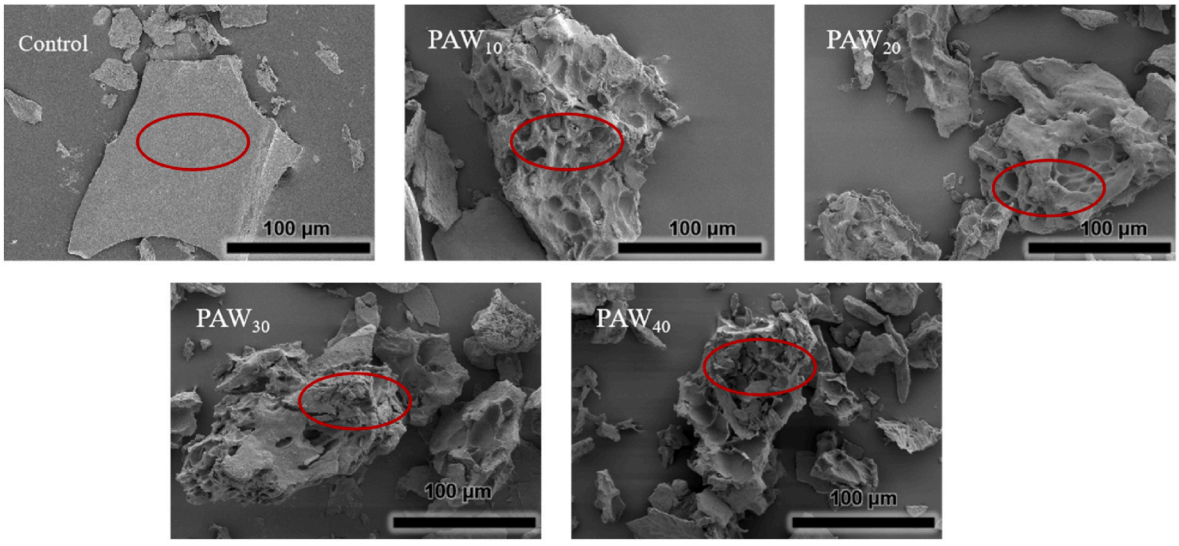

Fig. 5. Scanning electron micrographs of PSE-like chicken protein isolate treated with different plasma activation times.

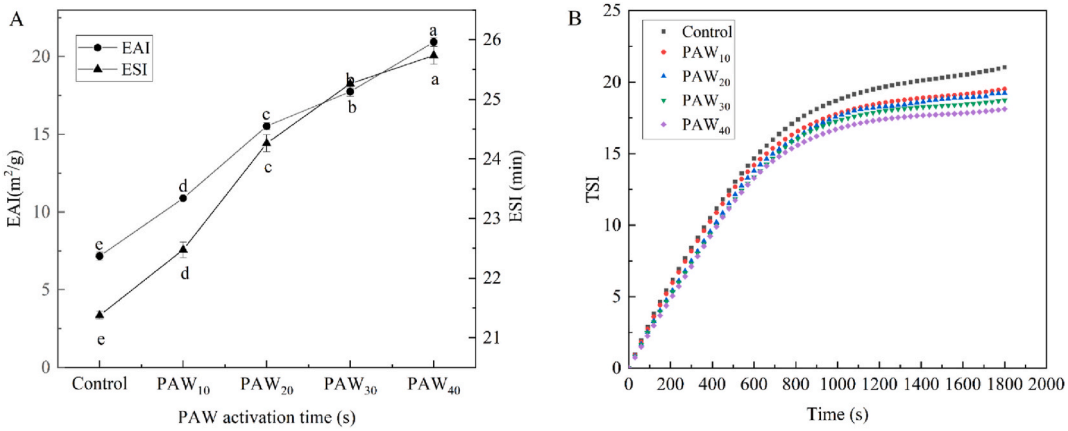

Fig. 6. Effect of plasma activation time on emulsifying activity index (EAI) and emulsifying stability index (ESI) and turbiscan stability index (TSI) of PSE-like chicken protein isolate. A: EAI and ESI, B: TSI. Different letters (a–e) indicate significant differences ($P < 0.05$).

3.12. Turbiscan stability index

TSI is a crucial parameter in evaluating the stability of emulsions and has a significant role in characterizing the instability of dispersion systems. A lower TSI value is indicative of greater system stability (Xiong and Sha, 2022). As illustrated in Fig. 6B, at the beginning of the determination, the TSI value of each sample rose rapidly with increasing determination time, then the increase speed began to slow down at 1000 s, and finally stabilized at 1800 s. During the given 1800 s period, the TSI value of PPI emulsion after PAW treatment was lower than those of the control, which indicated PAW could enhance the stability of PPI emulsion. Among them, the TSI of PPI emulsion after PAW_{40} treatment was the lowest, indicating that PPI emulsion was most stable when PAW_{40} was used. This result was in line with those of EAI and ESI (Fig. 6A). Zhao et al. (2023) found that plasma treatment caused to a decrease in the dynamic instability of emulsions of chickpea isolate proteins and more stable emulsions with increasing time.

3.13. In vitro protein digestibility and laser microconfocal Raman spectrometer

The protein digestibility rate serves as an indicator of the protein's susceptibility to hydrolysis and reflects nutritional properties (Duodu et al., 2003). As illustrated in Fig. 7A, IVPD significantly increased with increasing PAW activation time ($P < 0.05$). When the PAW activation time increased to 40 s, the IVPD of the protein increased by 25.15% ($P < 0.05$). This phenomenon was possibly attributed to the reactivity of the substances from PAW, leading to structural modifications in the protein. Consequently, this exposure reveals previously concealed cleavage sites within the natural protein structure, thereby facilitating accessibility for digestive enzymes and enhancing their digestibility (Olatunde et al., 2023). From the SEM results (Fig. 5), it could be seen that the protein surface roughness increased the contact area with the digestive enzymes, increased the number of enzyme-cutting sites, accelerates the digestive reaction, and improves the digestibility (Lazaro et al., 2018; Tian et al., 2017). Furthermore, Zhou et al. (2015) suggested that moderate oxidation energy increased the hydrophobicity and flexibility of the protein surface, thereby improving the digestibility of digestion. Wang et al. (2023) discovered plasma improved the digestibility of chickpea protein.

Microscopic images (Fig. 7B) can reflect the morphology of digested proteins, as well as the degree of protein degradation after digestion (Zhang et al., 2023). Microscopic images demonstrated that, throughout the entire simulated gastric-intestinal digestion process (3 h), protein particles in all sample groups, except for the control group, appeared smaller and more dispersed demonstrated to the control. Moreover, microscopic images of the digested sample treated with PAW showed a noticeable reduction in red fluorescent spots to control, indicating a higher level of protein degradation. These findings corroborate the results derived from digestibility assessments. In summary, at PAW_{40}, where PPI exhibited maximal digestibility, microscopic analysis demonstrated smaller and more uniformly dispersed protein particles. This observation aligns with prior digestibility results (Fig. 7A).

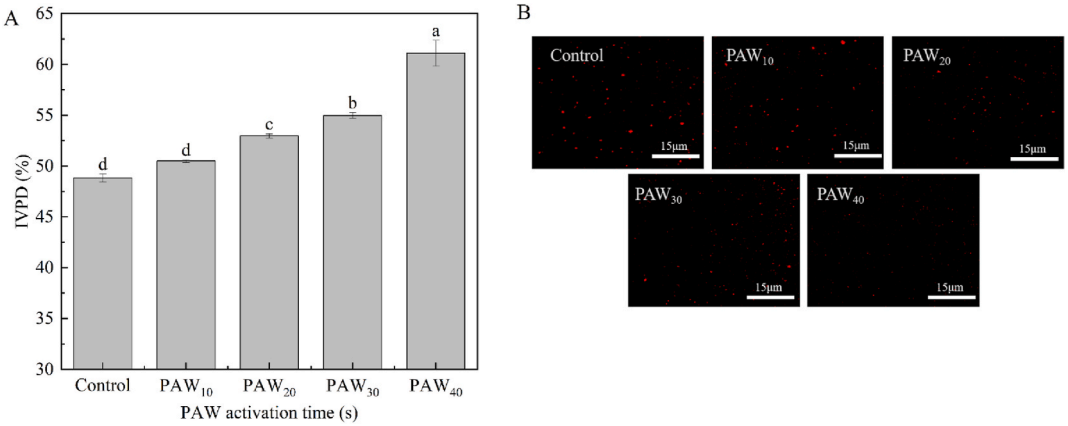

Fig. 7. Effect of plasma activation time on the digestibility and microscopic image of protein during simulated gastrointestinal digestion. A: protein digestibility, B: microscopic image. Different letters (a–d) indicate significant differences ($P < 0.05$).

4. Conclusions

PPI were treated with PAW for varying activation times. The results indicated that PAW treatment significantly increased the surface hydrophobicity of protein, which enhanced its binding to oil droplets. This, in turn caused to improvements in the EAI and ESI, and reduced in the TSI, and increased in the *in vitro* digestibility of protein. The above research showed that plasma activated water treatment changed the secondary structure of PPI, and improved the emulsification and digestive properties of PPI. A theoretical basis is provided for the development of easily digestible functional protein-based food for PSE-like chicken protein processing.

CRediT authorship contribution statement

Ke Li: Conceptualization, Methodology, Validation, Writing – review & editing, Writing – review & editing. **Yanfang Zhou:** Investigation, Data curation, Formal analysis, Writing – review & editing. **Chenyan Zhu:** Data curation, Formal analysis, Methodology, Validation. **Manting Du:** Investigation, Data curation, Visualization. **Bo Chen:** Supervision, Project administration. **Dianbo Zhao:** Conceptualization. **Yanhong Bai:** Conceptualization, Supervision, All authors have read and agreed to the published version of the manuscript.

Declaration of competing interest

The authors affirm that there are no identifiable conflicting financial interests or personal associations that may have seemed to exert an influence on the findings presented in this manuscript.

Acknowledgment

This research was supported by the National Natural Science Foundation of China (32372382), and Program for Science & Technology Innovation Talents in Universities of Henan Province (25HASTIT039).

Data availability

The authors do not have permission to share data.

References

Baron, C.P., Kjærsgård, I.V.H., Jessen, F., Jacobsen, C., 2007. Protein and lipid oxidation during frozen storage of rainbow trout (*Oncorhynchus mykiss*). J. Agric. Food Chem. 55, 8118–8125. https://doi.org/10.1021/jf070686f.

Carvalho, R.H., Soares, A.L., Honorato, D.C.B., Guarnieri, P.D., Pedrao, M.R., Paiao, F.G., Oba, A., Ida, E.I., Shimokomaki, M., 2014. The incidence of pale, soft, and exudative (PSE) Turkey meat at a Brazilian commercial plant and the functional properties in its meat product. LWT–Food Sci. Technol. 59, 883–888. https://doi.org/10.1016/j.lwt.2014.07.019.

Dabade, A., Kahar, S., Acharjee, A., Bhushette, P., Annapure, U., 2023. Effect of atmospheric pressure non-thermal pin to plate cold plasma on structural and functional properties of soy protein isolate. Journal of Agriculture and Food Research 12. https://doi.org/10.1016/j.jafr.2023.100538.

Duodu, K.G., Taylor, J.R.N., Belton, P.S., Hamaker, B.R., 2003. Factors affecting sorghum protein digestibility. J. Cereal. Sci. 38, 117–131. https://doi.org/10.1016/s0733-5210(03)00016-x.

Eazhumalai, G., Kalaivendan, R.G.T., Annapure, U.S., 2023. Effect of atmospheric pin-to-plate cold plasma on oat protein: structural, chemical, and foaming characteristics. Int. J. Biol. Macromol. 242, 15. https://doi.org/10.1016/j.ijbiomac.2023.125103.

Ekezie, F.G.C., Sun, D.W., Cheng, J.H., 2019a. Altering the IgE binding capacity of king prawn (*Litopenaeus Vannamei)* tropomyosin through conformational changes induced by cold argon-plasma jet. Food Chem. 300, 10. https://doi.org/10.1016/j.foodchem.2019.125143.

Ekezie, F.G.C., Cheng, J.H., Sun, D.W., 2019b. Effects of atmospheric pressure plasma jet on the conformation and physicochemical properties of myofibrillar proteins from king prawn (*Litopenaeus vannamei*). Food Chem. 276, 147–156. https://doi.org/10.1016/j.foodchem.2018.09.113.

Farooq, S., Dar, A.H., Dash, K.K., Srivastava, S., Pandey, V.K., Ayoub, W.S., Pandiselvam, R., Manzoor, S., Kaur, M., 2023. Cold plasma treatment advancements in food processing and impact on the physiochemical characteristics of food products. Food Sci. Biotechnol. 32, 621–638. https://doi.org/10.1007/s10068-023-01266-5.

Gao, X., Fan, X.K., Wang, Y., Liang, H.H., Li, A.X., Zhou, C.L., 2023. Individual effects of L-arginine and L-lysine on the physicochemical and textural properties of pale, soft and exudative-like emulsion sausage. Int. J. Food Sci. Technol. 58, 5874–5884. https://doi.org/10.1111/ijfs.16690.

Hadinoto, K., Niemira, B.A., Trujillo, F.J., 2023. A review on plasma-activated water and its application in the meat industry. Compr. Rev. Food Sci. Food Saf. 22, 4993–5019. https://doi.org/10.1111/1541-4337.13250.

Hatab, S., Koddy, J.K., Miao, W.H., Tang, L.L., Xu, H.Q., Deng, S.G., Zheng, B., 2022. Atmospheric cold plasma: a new approach to modify protein and lipid properties of myofibrillar protein isolate from hairtail (Trichiurus lepturus) fish. J. Sci. Food Agric. 102, 2041–2049. https://doi.org/10.1002/jsfa.11543.

Jadhav, H.B., Annapure, U., 2021. Consequences of non-thermal cold plasma treatment on meat and dairy lipids - a review. Future Foods 4, 12. https://doi.org/10.1016/j.fufo.2021.100095.

Jiang, W., Wu, R.A., Hu, X., Zhang, R.R., Ding, T., Zhou, J.W., 2023. Changes in physicochemical and conformational properties of myofibrillar proteins isolated from Mandarin fish (*Siniperca chuatsi*) treated by atmospheric pressure plasma jet. CyTA-J. Food 21, 625–633. https://doi.org/10.1080/19476337.2023.2264900.

Kang, C.D., Xiang, Q.S., Zhao, D.B., Wang, W.J., Niu, L.Y., Bai, Y.H., 2019. Inactivation of *Pseudomonas deceptionensis* CM2 on chicken breasts using plasma-activated water. J. Food Sci. Technol.-Mysore 56, 4938–4945. https://doi.org/10.1007/s13197-019-03964-7.

Lazaro, H., Puente, L., Zúñiga, M.C., Muñoz, L.A., 2018. Assessment of rheological and microstructural changes of soluble fiber from chia seeds during an *in vitro* micro-digestion. LWT–Food Sci. Technol. 95, 58–64. https://doi.org/10.1016/j.lwt.2018.04.052.

Li, F.F., Wang, B., Liu, Q., Chen, Q., Zhang, H.W., Xia, X.F., Kong, B.H., 2019. Changes in myofibrillar protein gel quality of porcine *longissimus* muscle induced by its stuctural modification under different thawing methods. Meat Sci. 147, 108–115. https://doi.org/10.1016/j.meatsci.2018.09.003.

Li, K., Fu, L., Zhao, Y.Y., Xue, S.W., Wang, P., Xu, X.L., Bai, Y.H., 2020a. Use of high-intensity ultrasound to improve emulsifying properties of chicken myofibrillar protein and enhance the rheological properties and stability of the emulsion. Food Hydrocoll. 98, 11. https://doi.org/10.1016/j.foodhyd.2019.105275.

Li, N., Yu, J.J., Jin, N., Chen, Y., Li, S.H., Chen, Y., 2020b. Modification of the physicochemical and structural characteristics of zein suspension by dielectric barrier discharge cold plasma treatment. J. Food Sci. 85, 2452–2460. https://doi.org/10.1111/1750-3841.15350.

Li, K., Li, S.Y., He, Y.Y., Wang, Y.Q., Zhang, Y.X., Zhao, Y.Y., Du, M.T., Wang, Y., Wang, Y.T., Bai, Y.H., 2022a. Application of ultrasound-assisted alkaline extraction for improving the solubility and emulsifying properties of pale, soft, and exudative (PSE)-like chicken breast meat protein isolate. LWT–Food Sci. Technol. 172, 10. https://doi.org/10.1016/j.lwt.2022.114234.

Li, M.Z., Shi, T., Wang, X., Bao, Y.L., Xiong, Z.Y., Monto, A.R., Jin, W.A., Yuan, L., Gao, R.C., 2022b. Plasma-activated water promoted the aggregation of Aristichthys nobilis myofibrillar protein and the effects on gelation properties. Curr. Res. Food Sci. 5, 1616–1624. https://doi.org/10.1016/j.crfs.2022.09.003.

Li, K., Wang, L.M., Gao, H.J., Du, M.T., Bai, Y.H., 2023. Use of basic amino acids to improve gel properties of PSE-like chicken meat proteins isolated via ultrasound-assisted alkaline extraction. J. Food Sci. 88, 5136–5148. https://doi.org/10.1111/1750-3841.16800.

Li, J.Q., Rao, W., Sun, Y.Y., Zhou, C.Y., Xia, Q., He, J., Pan, D.D., Du, L.H., 2024. Structural and gel property changes in chicken myofibrillar protein induced by argon cold plasma-activated water: with a molecular docking perspective. Food Res. Int. 197, 11. https://doi.org/10.1016/j.foodres.2024.115271.

Liao, X.Y., Xiang, Q.S., Cullen, P.J., Su, Y.A., Chen, S.G., Ye, X.Q., Liu, D.H., Ding, T., 2020. Plasma-activated water (PAW) and slightly acidic electrolyzed water (SAEW) as beef thawing media for enhancing microbiological safety. LWT–Food Sci. Technol. 117, 6. https://doi.org/10.1016/j.lwt.2019.108649.

Liu, H.T., Zhang, H., Liu, Q., Chen, Q., Kong, B.H., 2020. Solubilization and stable dispersion of myofibrillar proteins in water through the destruction and inhibition of the assembly of filaments using high-intensity ultrasound. Ultrason. Sonochem. 67, 11. https://doi.org/10.1016/j.ultsonch.2020.105160.

Luo, J., Xu, W.M., Liu, Q., Zou, Y., Wang, D.Y., Zhang, J.H., 2022. Dielectric barrier discharge cold plasma treatment of pork loin: effects on muscle physicochemical properties and emulsifying properties of pork myofibrillar protein. LWT–Food Sci. Technol. 162, 9. https://doi.org/10.1016/j.lwt.2022.113484.

Mehr, H.M., Koocheki, A., 2020. Effect of atmospheric cold plasma on structure, interfacial and emulsifying properties of Grass pea (*Lathyrus sativus* L.) protein isolate. Food Hydrocoll. 106, 16. https://doi.org/10.1016/j.foodhyd.2020.105899.

Miao, W.H., Nyaisaba, B.M., Koddy, J.K., Chen, M.L., Hatab, S., Deng, S.G., 2020. Effect of cold atmospheric plasma on the physicochemical and functional properties of myofibrillar protein from Alaska pollock (*Theragra chalcogramma*). Int. J. Food Sci. Technol. 55, 517–525. https://doi.org/10.1111/ijfs.14295.

Misra, N.N., Pankaj, S.K., Segat, A., Ishikawa, K., 2016. Cold plasma interactions with enzymes in foods and model systems. Trends Food Sci. Technol. 55, 39–47. https://doi.org/10.1016/j.tifs.2016.07.001.

Mollakhalili-Meybodi, N., Yousefi, M., Nematollahi, A., Khorshidian, N., 2021. Effect of atmospheric cold plasma treatment on technological and nutrition functionality of protein in foods. Eur. Food Res. Technol. 247, 1579–1594. https://doi.org/10.1007/s00217-021-03750-w.

Olatunde, O.O., Benjakul, S., Vongkamjan, K., 2019. Combined effects of high voltage cold atmospheric plasma and antioxidants on the qualities and shelf-life of Asian sea bass slices. Innov. Food Sci. Emerg. Technol. 54, 113–122. https://doi.org/10.1016/j.ifset.2019.03.012.

Olatunde, O.O., Hewage, A., Dissanayake, T., Aluko, R.E., Karaca, A.C., Shang, N., Bandara, N., 2023. Cold atmospheric plasma-induced protein modification: novel nonthermal processing technology to improve protein quality, functionality, and allergenicity reduction. Compr. Rev. Food Sci. Food Saf. 22, 2197–2234. https://doi.org/10.1111/1541-4337.13144.

Owens, C.M., Hirschler, E.M., McKee, S.R., Martinez-Dawson, R., Sams, A.R., 2000. The characterization and incidence of pale, soft, exudative Turkey meat in a commercial plant. Poult. Sci. 79, 553–558. https://doi.org/10.1093/ps/79.4.553.

Park, D., Xiong, Y.L.L., Alderton, A.L., 2007. Concentration effects of hydroxyl radical oxidizing systems on biochemical properties of porcine muscle myofibrillar protein. Food Chem. 101, 1239–1246. https://doi.org/10.1016/j.foodchem.2006.03.028.

Qian, J., Wang, Y.Y., Zhuang, H., Yan, W.J., Zhang, J.H., Luo, J., 2021. Plasma activated water-induced formation of compact chicken myofibrillar protein gel structures with intrinsically antibacterial activity. Food Chem. 351, 8. https://doi.org/10.1016/j.foodchem.2021.129278.

Rao, W., Roopesh, M.S., Pan, D.D., Du, L.H., 2023. Enhanced gel properties of duck myofibrillar protein by plasma-activated water: through mild structure modifications. Foods 12, 17. https://doi.org/10.3390/foods12040877.

Sarangapani, C., Misra, N.N., Milosavljevic, V., Bourke, P., O'Regan, F., Cullen, P.J., 2016. Pesticide degradation in water using atmospheric air cold plasma. J. Water Process Eng. 9, 225–232. https://doi.org/10.1016/j.jwpe.2016.01.003.

Segat, A., Misra, N.N., Cullen, P.J., Innocente, N., 2016. Effect of atmospheric pressure cold plasma (ACP) on activity and structure of alkaline phosphatase. Food Bioprod. Process. 98, 181–188. https://doi.org/10.1016/j.fbp.2016.01.010.

Sharafodin, H., Soltanizadeh, N., 2022. Potential application of DBD plasma technique for modifying structural and physicochemical properties of soy protein isolate. Food Hydrocoll. 122, 16. https://doi.org/10.1016/j.foodhyd.2021.107077.

Sharifian, A., Soltanizadeh, N., Abbaszadeh, R., 2019. Effects of dielectric barrier discharge plasma on the physicochemical and functional properties of myofibrillar proteins. Innov. Food Sci. Emerg. Technol. 54, 1–8. https://doi.org/10.1016/j.ifset.2019.03.006.

Soladoye, O.P., Juarez, M.L., Aalhus, J.L., Shand, P., Estévez, M., 2015. Protein oxidation in processed meat: mechanisms and potential implications on human health. Compr. Rev. Food Sci. Food Saf. 14, 106–122. https://doi.org/10.1111/1541-4337.12127.

Sun, F.S., Xie, X.X., Zhang, Y.F., Ma, M.Y., Wang, Y.Q., Duan, J.W., Lu, X.P., Yang, G.X., He, G.Y., 2021. Wheat gliadin in ethanol solutions treated using cold air plasma at atmospheric pressure. Food Biosci. 39, 11. https://doi.org/10.1016/j.fbio.2020.100808.

Sun, B.L., Zhang, P.X., Zhang, J.J., Huang, T., Li, C., Yang, W.E., 2022. Preparation, characterization and bioavailability studies of Tegillarca granosa hemoglobin and its glycosylated products. Int. J. Biol. Macromol. 219, 11–20. https://doi.org/10.1016/j.ijbiomac.2022.07.234.

Tian, Y.Y., Wang, W., Yuan, C.H., Zhang, L., Liu, J.Y., Liu, J.R., 2017. Nutritional and digestive properties of protein isolates extracted from the muscle of the common carp using pH-shift processing. J. Food Process. Preserv. 41, 9. https://doi.org/10.1111/jfpp.12847.

Ukai, T., Matsumura, Y., Urade, R., 2008. Disaggregation and reaggregation of gluten proteins by sodium chloride. J. Agric. Food Chem. 56, 1122–1130. https://doi.org/10.1021/jf0725676.

Visessanguan, W., Ogawa, M., Nakai, S., An, H., 2000. Physicochemical changes and mechanism of heat-induced gelation of arrowtooth flounder myosin. J. Agric. Food Chem. 48, 1016–1023. https://doi.org/10.1021/jf9900332.

Wang, H.B., Pei, Z.S., Xue, C.F., Cao, J., Shen, X.R., Li, C., 2022a. Comparative study on the characterization of myofibrillar proteins from Tilapia, golden pompano and skipjack tuna. Foods 11, 13. https://doi.org/10.3390/foods11121705.

Wang, Y.T., Wang, S.S., Li, R., Wang, Y.J., Xiang, Q.S., Li, K., Bai, Y.H., 2022b. Effects of combined treatment with ultrasound and pH shifting on foaming properties of chickpea protein isolate. Food Hydrocoll. 124, 10. https://doi.org/10.1016/j.foodhyd.2021.107351.

Wang, J., Zhou, X.Y., Ju, S.L., Cai, R.Y., Roopesh, M.S., Pan, D.D., Du, L.H., 2023. Influence of atmospheric pressure plasma jet on the structural, functional and digestive properties of chickpea protein isolate. Food Res. Int. 174, 11. https://doi.org/10.1016/j.foodres.2023.113565.

Wang, J., Zhou, X.Y., Li, J.Q., Pan, D.D., Du, L.H., 2024. Enhancing the functionalities of chickpea protein isolate through a combined strategy with pH-shifting and cold plasma treatment. Innov. Food Sci. Emerg. Technol. 93, 11. https://doi.org/10.1016/j.ifset.2024.103607.

Wierenga, P.A., Meinders, M.B.J., Egmond, M.R., Voragen, F., de Jongh, H.H.J., 2003. Protein exposed hydrophobicity reduces the kinetic barrier for adsorption of ovalbumin to the air-water interface. Langmuir 19, 8964–8970. https://doi.org/10.1021/la034868p.

Xiong, Y.L., Sha, L., 2022. Comparative structural and emulsifying properties of ultrasound-treated pea (Pisum sativum L.) protein isolate and the legumin and vicilin fractions. Food Res. Int. 156, 9. https://doi.org/10.1016/j.foodres.2022.111179.

Xiong, Y.L., Blanchard, S.P., Ooizumi, T., Ma, Y.Y., 2010. Hydroxyl radical and ferryl-generating systems promote gel network formation of myofibrillar protein. J. Food Sci. 75, C215–C221. https://doi.org/10.1111/j.1750-3841.2009.01511.x.

Yang, Z.Y., Sun, J., Li, Z., Qi, Y., Wang, P., Xu, X.L., 2021. Robustness of protein: using pH shifting and low speed shearing to partially recover conformation and dispersibility of myosin from pale, soft, exudative (PSE)-like chicken breast. LWT–Food Sci. Technol. 138, 9. https://doi.org/10.1016/j.lwt.2020.110786.

Yang, T.L., Zhang, H., Bian, Y.Q., Qu, Z.H., Zhang, Y.F., Li, S.H., Chen, G.Y., Chen, Y., 2025. Ultrasonic-assisted plasma-activated water extraction of polysaccharide from *Hemerocallis citrina* Baroni: structural characterization and antioxidant mechanism *in vitro*. Food Chem. 465, 12. https://doi.org/10.1016/j.foodchem.2024.142049.

Yu, X., Huang, S.S., Nie, C.Z., Deng, Q.C., Zhai, Y.F., Shen, R.L., 2020. Effects of atmospheric pressure plasma jet on the physicochemical, functional, and antioxidant properties of flaxseed protein. J. Food Sci. 85, 2010–2019. https://doi.org/10.1111/1750-3841.15184.

Yu, J.J., Jiang, P.Y., Li, S.H., Chen, Y., 2022. Mechanism of improving interfacial hydration characteristic of high-denatured peanut protein induced by cold plasma. J. Food Process. Eng. 45, 12. https://doi.org/10.1111/jfpe.13926.

Zhang, W.G., Xiao, S., Ahn, D.U., 2013. Protein oxidation: basic principles and implications for meat quality. Crit. Rev. Food Sci. Nutr. 53, 1191–1201. https://doi.org/10.1080/10408398.2011.577540.

Zhang, Z.Y., Yang, Y.L., Zhou, P., Zhang, X., Wang, J.Y., 2017. Effects of high pressure modification on conformation and gelation properties of myofibrillar protein. Food Chem. 217, 678–686. https://doi.org/10.1016/j.foodchem.2016.09.040.

Zhang, Y.M., Lv, Y.Q., Chen, L., Wu, H.Z., Zhang, Y.Y., Suo, Z.Y., Wang, S.X., Liang, Y.X., Xu, X.L., Zhou, G.H., Feng, X.C., 2018. Inhibition of epigallocatechin-3-gallate/protein interaction by methyl-β-cyclodextrin in myofibrillar protein emulsion gels under oxidative stress. J. Agric. Food Chem. 66, 8094–8103. https://doi.org/10.1021/acs.jafc.8b00275.

Zhang, W.W., Liu, C.Q., Zhao, J., Ma, T.Y., He, Z.D., Huang, M.G., Wang, Y.S., 2021. Modification of structure and functionalities of ginkgo seed proteins by pH-shifting treatment. Food Chem. 358, 8. https://doi.org/10.1016/j.foodchem.2021.129862.

Zhang, F.X., Yue, Q., Li, X., Kong, B.H., Sun, F.D., Cao, C.A., Zhang, H.W., Liu, Q., 2023. Mechanisms underlying the effects of ultrasound-assisted alkaline extraction on the structural properties and *in vitro* digestibility of *Tenebrio molitor* larvae protein. Ultrason. Sonochem. 94, 11. https://doi.org/10.1016/j.ultsonch.2023.106335.

Zhao, X., Xing, T., Chen, X., Han, M.Y., Deng, S.L., Xu, X.L., Zhou, G.H., 2017. Changes of molecular forces during thermo-gelling of protein isolated from PSE-like chicken breast by various isoelectric solubilization/precipitation extraction strategies. Food Bioprocess Technol. 10, 1240–1247. https://doi.org/10.1007/s11947-017-1893-4.

Zhao, X., Bai, Y., Xing, T., Xu, X.L., Zhou, G.H., 2018. Use of an isoelectric solubilization/precipitation process to modify the functional properties of PSE (pale, soft, exudative)-like chicken meat protein: a mechanistic approach. Food Chem. 248, 201–209. https://doi.org/10.1016/j.foodchem.2017.12.048.

Zhao, X., Xing, T., Xu, X.L., Zhou, G.H.G., 2020. Influence of extreme alkaline pH induced unfolding and aggregation on PSElike chicken protein edible film formation. Food Chem. 319, 10. https://doi.org/10.1016/j.foodchem.2020.126574.

Zhao, C.B., Miao, Z.C., Yan, J.N., Liu, J., Chu, Z.J., Yin, H.H., Zheng, M.Z., Liu, J.S., 2022. Ultrasound-induced red bean protein-lutein interactions and their effects on physicochemical properties, antioxidant activities and digestion behaviors of complexes. LWT–Food Sci. Technol. 160, 10. https://doi.org/10.1016/j.lwt.2022.113322.

Zhao, D.B., Zhou, Y.F., Sun, L.X., Tian, J.F., Xiang, Q.S., Li, K., 2023. The stability, rheological properties and interfacial properties of oil-in-water (O/W) emulsions prepared from dielectric barrier discharge (DBD) cold plasma-treated chickpea protein isolate and myofibrillar protein complexes. Foods 12, 17. https://doi.org/10.3390/foods12193629.

Zhou, F.B., Zhao, M.M., Cui, C., Sun, W.Z., 2015. Influence of linoleic acid-induced oxidative modifications on physicochemical changes and *in vitro* digestibility of porcine myofibrillar proteins. LWT–Food Sci. Technol. 61, 414–421. https://doi.org/10.1016/j.lwt.2014.12.037.